Results in Chemistry 4 (2022) 100388

Contents lists available at ScienceDirect

Results in Chemistry

journal homepage: www.sciencedirect.com/journal/results-in-chemistry

NIR-emission from Yb(III)- and Nd(III)-based complexes in the solid state sensitized by a ligand system absorbing in a broad UV and visible spectral window

Enrico Cavalli [a], Silvia Ruggieri [b], Silvia Mizzoni [b], Chiara Nardon [b], Marco Bettinelli [b], Fabio Piccinelli [b,*]

[a] Department of Chemical Sciences, Life and Environmental Sustainability, Parma University, viale delle Scienze 17/a, 43124 Parma, Italy
[b] Luminescent Materials Laboratory, DB, University of Verona, and INSTM, UdR Verona, Strada Le Grazie 15, 37134 Verona, Italy

ARTICLE INFO

Keywords:
Coordination chemistry
NIR luminescence
Lanthanide ion
Solid state
ligand-to-metal charge transfer (LMCT) band
Chromophoric ligand

ABSTRACT

In this contribution, we present the synthesis, characterization and spectroscopic investigation of the heteroleptic (*R,R*)-Yb**L1**(tta) and (*R,R*)-Nd**L1**(tta) complexes (with *tta* = 2-thenoyltrifluoroacetonate and **L1** = N,N′-bis(2-(8-hydroxyquinolinate)methylidene)-1,2-(R,R or S,S)-cyclohexanediamine) in the solid state. The *f-f* metal-centered NIR luminescence emission of Nd(III) and Yb(III) is efficiently sensitized by both chromophoric ligands in a very broad range of wavelengths [from 250 to 600 nm, in the case of Nd(III) and from 250 to 650 nm, for Yb(III)]. A possible energy transfer mechanism is proposed: for (*R,R*)-Nd**L1**(tta) complex a classical Ligand-to-Metal Energy Transfer (LMET) mechanism (*antenna effect*) is suggested, whilst in the case of the (*R,R*)-Yb**L1**(tta) complex, the presence of a ligand-to-metal charge transfer (LMCT) state determines the sensitization of Yb(III) luminescence. We propose that this level is populated by the singlet and triplet excited states belonging to $\pi \rightarrow \pi^*$ and $n \rightarrow \pi^*$ transitions of both ligands and it can transfer the excitation energy to $^2F_{5/2}$.

Introduction

Near-infrared (NIR) lanthanide-based luminescent coordination compounds have attracted increasing attention, for example, as luminescent probes for cell imaging and medical diagnostics, [1–6] due to their favourable emission in the so-called second biological window (1000–1400 nm range) where the tissues are quite transparent and the photons can penetrate deeply into samples. Therefore, the Nd(III) and Yb(III) ions, possessing NIR luminescence (the former around 900 and 1060 nm; the latter around 980 nm), are associated with extensive application prospects in bioanalytical field. to increase the luminescence intensity of a Ln(III) ion a ligand-to-metal energy transfer (LMET or *antenna effect*) process is Usually, exploited. In fact, since upon direct excitation of the Ln(III) ion only a weak luminescence emission can be obtained, the strong absorption of the excitation light by the organic ligand, followed by the transfer of energy to the metal ion, can ensure high values of *brightness*.[7] The coordination of the metal ion by at least an organic ligand usually leads to another beneficial effect, as the inner coordination sphere of the cation is protected by the intrusion of solvent molecules. Such molecules, like in the case of water as a solvent, can possess high energy vibrations (*i.e.*, O—H groups) which are known to strongly reduce the Ln(III) luminescence efficiency, by means of multiphonon relaxation (MPR) processes.[8,9] Based on the Dexter's theory of nonradiative energy transfer (ET), [10] the ET efficiency is optimal when the spectral overlap of the emission band of the donor (D, the ligand in our case) and the absorption band of the acceptor (A, the lanthanide ion in our case) is maximized and when the D-A distance is small. In other words, the excited levels of the ligand involved in the ET mechanism (usually singlet and triplet states) should be close in energy to the excited states of the lanthanide ion. Taking into account the energy level diagram of the Ln(III) ions reported by Dieke *et al.* [11,12], in the case of Nd(III) the $^4F_{3/2}$ NIR emitting level can be populated by energy transfer from an excited state of the ligand located in the NIR around 12000 cm^{-1}. Alternatively, ligand excited states located in the UV/Vis region can populate the dense series of Nd(III) levels at energy above 12000 cm^{-1}, which can then relax to $^4F_{3/2}$ by MPR. If the excitation of Nd(III) through a chromophoric ligand seems not so difficult, the presence of only one excited level ($^2F_{5/2}$) in the case of Yb(III)

* Corresponding author.
E-mail address: fabio.piccinelli@univr.it (F. Piccinelli).

https://doi.org/10.1016/j.rechem.2022.100388
Received 30 March 2022; Accepted 31 May 2022
Available online 2 June 2022

represents a limitation for the excitation of this ion by means of a LMET process. Therefore, often, the sensitization of the Yb(III) emission cannot be accounted for in the frame of the classical Dexter theory, as a consequence of the large mismatch between the involved electronic levels of the ligand and Yb(III). So far, three mechanisms have been invoked in this connection. The first one occurs by an internal redox process involving the Yb(III)/Yb(II) redox couple and the excited state of the ligand [13] while the second by an internal conversion inside the energy levels of the Yb(III)-ligand system considered as a single chromophore.[14] The third mechanism foresees the involvement of a Ligand-to-Metal Charge Transfer (LMCT) state.[15–17].

Recently, E. Kasprzycka et al. [18] proposed a $S_1 \rightarrow LMCT \rightarrow T_1 \rightarrow Yb^{3+}$ pathway on the basis of the energy transfer mechanism in Yb(III) complex with *N*-phosphorylated sulfonamide.

In this contribution, we present the synthesis, characterization and spectroscopic investigation in the solid state of two new heteroleptic complexes of Nd(III) and Yb(III) (Fig. 1) containing two chromophoric organic ligands (*tta* = 2-thenoyltrifluoroacetonate and H_2**L1** = *N,N′*-bis (2-(8-hydroxyquinolin)methylidene)-1,2-(R,R or S,S)-cyclohexanedia mine).

The intense and complementary absorption bands of the two ligands in the UV/Vis spectral region are involved in the efficient sensitization of the luminescence of both Ln(III) cations, which occurs in a broad spectral range (from 250 to 600/650 nm). In particular, for the Yb(III)-based complex, the involvement of a LMCT seems to play a pivotal role in the sensitization mechanism. As the complexes are chiral, thanks to the presence of the 1,2-(*R,R* or *S,S*)-cyclohexanediamine ring, their chiroptical properties [*i.e.,* Circularly Polarized Luminescence (CPL)] will be further investigated.

Materials and methods

General

$Yb(CH_3COO)_3$ and $Nd(CH_3COO)_3$ (Aldrich, 98 %) were stored under vacuum for several days at 80 °C and then transferred in a glove box. 2-Thenoyltrifluoroacetyl-acetone (Htta, Alfa Aesar, 98 %), 8-Hydroxy-2-quinolinecarboxaldehyde (Aldrich, 98 %), *trans-(R,R* or *S,S)*-1,2-diamminocyclohexane (Alfa Aesar, 98 %) and KOH in pellets (Fluka, 87 %) were used as received. Ethanol (Merck, 99.8 %), dichloromethane (Honeywell, 99.9 %), hexane (Honeywell, 99 %) were used as received. TLC plates on silica were purchased by Aldrich.

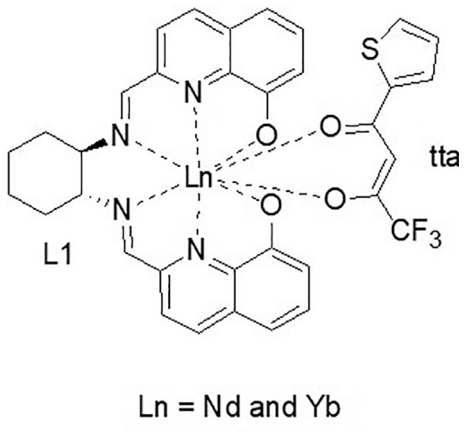

Fig. 1. Molecular structure of the complexes discussed in this contribution [(*R, R*)-Yb**L1**(tta) and (*R,R*)-Nd**L1**(tta)]. The *R,R* isomer of the $\mathbf{L1}^{2-}$ ligand is reported but both the enantiomeric complexes have been synthesized and studied.

Synthesis of the ligand H_2*L1*

At room temperature, in a round-bottom flask containing an ethanol solution (11 mL) of 8-Hydroxy-2-quinolinecarboxaldehyde (1.04 g, 6.01 mmol) was slowly added to *trans-(R,R* or *S,S)*-1,2-diamminocyclohexane (0.342 g, 3.00 mmol), previously dissolved in ethanol (7 mL). The obtained yellowish suspension was stirred for 4 h at 60 °C. The reaction was monitored by TLC on silica (hexane:DCM 70:30 v/v, as an eluent) to check the disappearance of the starting aldehyde ($R_f = 0.2$). Then, the suspension was filtered and the solid collected [1.12 g of ligand $\mathbf{H_2L1}$, pale yellow solid (Figure S1), 88 % chemical yield] after washing with a few mL of ethanol and drying. ^{1}H NMR (400 MHz, $CDCl_3$) δ (ppm): 8.45 (s, 2H, N = CH), 8.06 (m, 4H, Aromatics), 7.39 (t, *J* = 8 Hz, 2H), 7.25 (d, *J* = 8.3 Hz, 2H), 7.09 (d, *J* = 7.7 Hz, 2H), 3.66 – 3.59 (m, 2H, Cy, –CCH-N), 2.03 – 1.83 (m, 6H, Cy), 1.67 – 1.52 (m, 2H, Cy).

^{13}C NMR ($CDCl_3$) δ (ppm): 161.54 (C═N), 152.48 (-C-OH), 152.29 (-C-Ar), 137.49 (-C-Ar), 136.43 (-C-Ar), 128.90 (–CH-Ar), 128.54 (-C-Ar), 119.01 (–CH-Ar), 117.83 (–CH-Ar), 110.23 (–CH-Ar), 73.76 (Cy-CH), 32.73 (Cy-CH_2), 24.38 (Cy-CH_2).

*Synthesis of Yb*L1*(tta) and Nd*L1*(tta) complexes*

At room temperature, Htta = 2-thenoyltrifluoroacetone (0.052 g, 0.234 mmol) was dissolved in an ethanol (3 mL) solution containing 1.2 eq (0.0158 g, 0.28 mmol) of KOH. This mixture was added to a solution containing the ligand $\mathbf{H_2L1}$ (0.100 g, 0.234 mmol) and $Yb(CH_3COO)_3$ (0.082 g, 0.234 mmol) or $Nd(CH_3COO)_3$ (0.075 g, 0.234 mmol) in EtOH (8 mL). The final mixture was stirred at room temperature for 1 h. The solution volume was reduced to 2 mL under vacuum, 10 mL of dichloromethane (DCM) were added and the inorganic salt (CH_3COOK) was removed upon filtration. 0.150 – 0.165 g (yield around 85 %) of an orange [in the case of Nd(III)] or red [Yb(III)] solid (Figure S1), with a good degree of purity, were obtained after the complete evaporation of the solvent.

Elemental Anal. Calc. for Yb**L1**(tta) $C_{34}H_{26}F_3N_4O_4SYb$ (MW 816.69): C, 50.00; H, 3.21; N, 6.86; S, 3.93. Found (*R,R* isomer): C, 49.37; H, 3.75; N, 6.31; S, 3.46; (*S,S* isomer): C, 49.30; H, 3.78; N, 6.30; S, 3.41 ESI-MS (Scan ES+; *m/z*): 690.19 (100 %), 691.19 (40 %), 689.19 (66 %), for the $[Yb\mathbf{L1}(CH_3OH)_3]^+$ species; (Scan ES$^-$; *m/z*): 220.98 (100 %) for [tta]$^-$. IR (ATR; cm^{-1}, *R,R* isomer): 3050, 2933, 2860 (C—H stretching of **L1**); 1683, 1433 (ring stretching of **L1**); 1647 (imine C═N stretching); 1607, 1538 (tta carbonyl stretching); 1307 (C—O stretching of **L1**); 1084, 719 (skeleton in plane bending of **L1**).

Elemental Anal. Calc. for Nd**L1**(tta) $C_{34}H_{26}F_3N_4NdO_4S$ (MW 787.89): C, 51.83; H, 3.33; N, 7.11; S, 4.07. Found (*R,R* isomer): C, 52.23; H, 3.45; N, 7.14; S, 4.22; (*S,S* isomer): C, 52.19; H, 3.44; N, 7.20; S, 4.35. ESI-MS(Scan ES$^+$; *m/z*): 660.16 (100 %), 662.16 (90 %), 664.17 (80 %), 661.16 (80 %), for the $[Nd\mathbf{L1}(CH_3OH)_3]^+$ species; (Scan ES$^-$; *m/z*): 220.98 (100 %) for [tta]$^-$. IR (ATR; cm^{-1}, *R,R* isomer): 3050, 2936, 2862 (C—H stretching of **L1**); 1708, 1435 (ring stretching of **L1**); 1647 (imine C═N stretching); 1608, 1534 (tta carbonyl stretching); 1304 (C—O stretching of **L1**); 1094, 720 (skeleton in plane bending of **L1**).

NMR spectroscopy

Nuclear magnetic resonance (NMR) experiments (^{1}H and ^{13}C) were performed at 298.15 K using a 600 MHz Bruker Avance III spectrometer equipped with a triple resonance TCI cryogenic probe. Spectra were usually recorded in $CDCl_3$ and, unless otherwise stated, chemical shifts are expressed as ppm and referenced to the internal standard tetramethylsilane (TMS). One dimensional NMR spectra were recorded with 8 or 16 scans and a spectral width of 12019 Hz. All spectra were manually phased and baseline corrected using TOPSPIN 3.2 (Bruker, Karlsruhe, Germany). Chemical shift, multiplicity (s, singlet; d, doublet; t, triplet; m, multiplet; b, broad), coupling constants and integration area are reported.

Luminescence and decay kinetics

The emission and decay time measurements were carried out by means of an Edinburgh FLS1000 spectrofluorometer equipped with both continuous and pulsed Xe lamp, a double excitation monochromator, a single emission monochromator and a N_2-cooled NIR extended photomultiplier for the detection of the emitted signal. All the spectra were measured at room temperature and corrected for the spectral responsiveness of the setup. The pulse duration of the Xenon lamp is in the 1–2 s range.

ESI-MS

Electrospray ionization mass spectra (ESI-MS) were recorded with a Finnigan LXQ Linear Ion Trap (Thermo Scientific, San Jose, CA, USA) operating in positive ion mode. The data acquisition was under the control of Xcalibur software (Thermo Scientific). A CH_3OH solution of each sample was properly diluted and infused into the ion source at a flow rate of 10 μL/min with the aid of a syringe pump. The typical source conditions were: transfer line capillary at 275 °C; ion spray voltage at 4.70 kV; sheath, auxiliary and sweep gas (N_2) flow rates at 10, 5 and 0 arbitrary units, respectively. Helium was used as the collision damping gas in the ion trap set at a pressure of 1 mTorr.

Elemental analysis

Total carbon, hydrogen, nitrogen and sulphur concentrations were determined by flash combustion using an Elemental Analyser (CHNS vario Macro Cube, Elementar, Germany). Sulphanilamide (Elementar Analysensysteme GmbH, Germany) was used as a standard. The QA/QC was generally > 96 % for all elements.

Infrared spectroscopy

The infrared absorption spectra in the medium IR region were collected by means of a spectrophotometer Perkin-Elmer FT-IR Spectrum Two.

Results

*Spectroscopic characterization of (R,R)-Yb**L1**(tta)*

The excitation spectrum of the (*R,R*)-Yb**L1**(tta) complex with emission wavelength 976 nm is reported in Fig. 2. As the same spectrum recorded for the (*S,S*) enantiomer is identical it will be neither reported nor further discussed. Upon monitoring the Yb(III) emission, around the sharp band peaking at 976 nm and involving the lowest energy components (zero-line) of the $^2F_{5/2}$ and $^2F_{7/2}$ levels, a broad excitation band ranging from 250 to 650 nm was detected. This band seems made up of several components and the maximum of this group of bands is in the blue spectral region around 420 nm.

Upon excitation at 420 nm, the Yb(III) luminescence emission spectrum in the NIR range is shown in Fig. 3. It consists of a sharp zero-line peaking at 976 nm and a manifold in the 900–1100 nm region, associated to the crystal field splitting of the Yb(III) $^2F_{7/2}$ ground state.

The luminescence decay curve of the $^2F_{5/2}$ excited level of Yb(III) (at 976 nm) is reported in Fig. 4, upon excitation in the ligand absorption band (at 420 nm) (see below).

The decay profile of the emission presents a build-up and can be reliably reproduced by a difference of two exponential functions. Any conclusions about the origin of the rise-time cannot be considered reliable, as the related time constant [1.3(2) μs] is equal to the duration of the exciting lamp pulse. On the other hand, the time constant of the tail, 9.63(7) μs (R-Square 0.99815), is the lifetime of the $^2F_{5/2}$ excited state.

*Spectroscopic characterization of Nd**L1**(tta)*

The luminescence excitation spectrum of the (*R,R*)-Nd**L1**(tta) complex is shown in Fig. 5 (emission wavelength 1060 nm). Similarly to the Yb(III)-counterpart, the related spectrum of the (*S,S*) isomer is not reported since it is completely superimposable to that of its enantiomer.

In the excitation spectrum several features are clearly evident: a broad and dominant band in the 250–600 nm range, whose maximum intensity is twice that of Nd(III) excitation peaks located from 625 to 820 nm. Two main components (peaking at 375 nm and 490 nm, respectively) and a shoulder (at 580 nm) can be detected in the broad excitation band. All the narrow Nd(III) excitation peaks, located in the Vis/NIR spectral range, belong to transitions which involve the $^4I_{9/2}$ ground state of Nd(III) and several excited states, namely $^2H_{11/2}$, $^2H_{9/2}$, $^4F_{9/2}$, $^4F_{7/2}$, $^4F_{5/2}$ and $^4S_{3/2}$, as reported in Fig. 5.

The luminescence emission spectrum of (*R,R*)-Nd**L1**(tta) is reported in Fig. 6. Upon excitation at the maximum of the ligand absorption band (at 490 nm), the Nd(III) typical emission peaks in the NIR spectral range are observed. These bands result from the decay of the $^4F_{3/2}$ excited state on different ^4I_J levels (with J = 9/2, 11/2 and 13/2).

Upon excitation at 740 nm, no reliable luminescence decay curve was recorded in correspondence of the $^4F_{3/2} \rightarrow {}^4I_{11/2}$ transition of Nd (III), around 1060 nm. We can tentatively conclude that the $^4F_{3/2}$

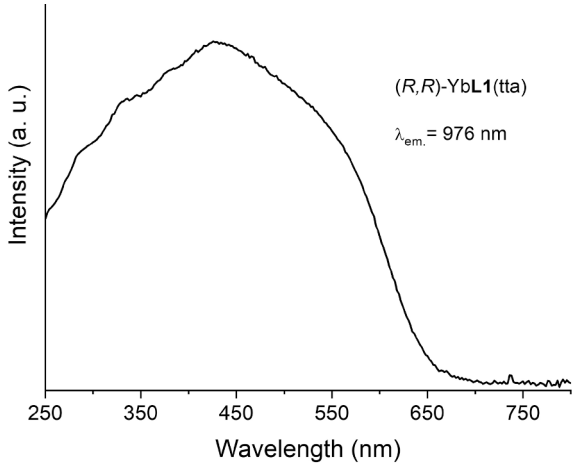

Fig. 2. Luminescence excitation spectrum of (*R,R*)-Yb**L1**(tta) in the solid state at room temperature (λ_{em} = 976 nm).

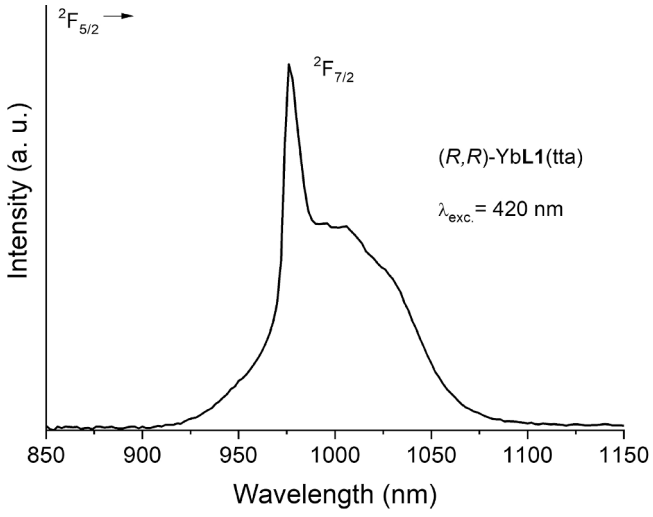

Fig. 3. Luminescence emission spectrum of (*R,R*)-Yb**L1**(tta) in the solid state at room temperature (λ_{exc} = 420 nm).

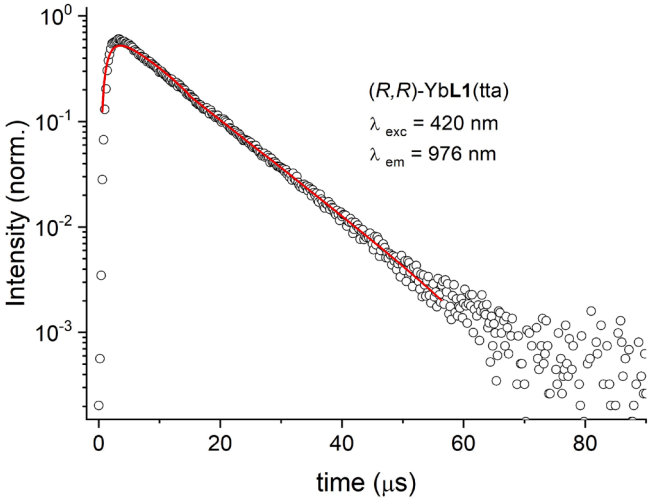

Fig. 4. Decay curve of the $^2F_{5/2}$ excited state of Yb(III) upon pulsed excitation in the case of (*R,R*)-Yb**L1**(tta) complex, in the solid state and at room temperature (λ_{exc} = 420 nm; λ_{em} = 976 nm).

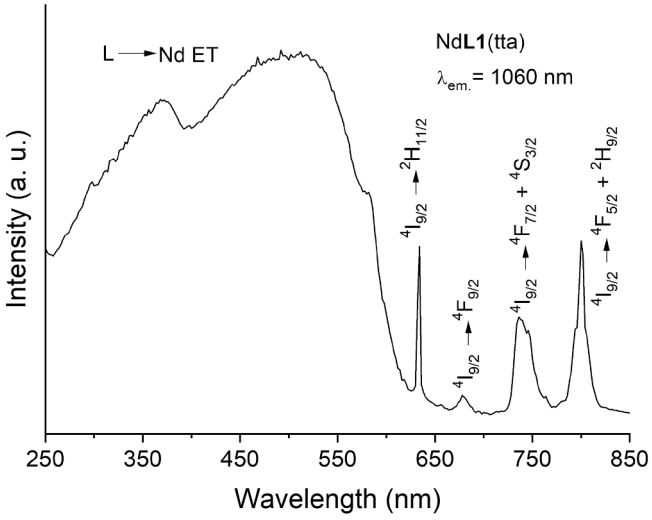

Fig. 5. Luminescence excitation spectrum of (*R,R*)-Nd**L1**(tta) in the solid state at room temperature (λ_{em} = 1060 nm).

lifetime of (*R,R*)-Nd**L1**(tta) is similar or shorter than the time duration of the pulse of the Xenon lamp used for the decay curve measurements.

Nature of the excitation transitions

In the absence of diffuse reflectance spectra on solid samples, due to the lack of suitable equipment, in order to understand the nature of transitions involved in the sensitization of the Ln(III) luminescence, UV–vis absorption spectra have been recorded in ethanol solutions. In particular, we collected spectra for (*R,R*)-Yb**L1**(tta), (*R,R*)-Nd**L1**(tta) complexes and the H_2**L1** ligand after addition of up to 2 equivalents of KOH with respect to the ligand. In the latter case, a strong absorption band in the UV region peaking at about 260 nm (ε = 71150 $L{\cdot}cm^{-1}{\cdot}mol^{-1}$) and two weak bands located around 305 (ε = 6850 $L{\cdot}cm^{-1}{\cdot}mol^{-1}$1) and 352 nm (ε = 3386 $L{\cdot}cm^{-1}{\cdot}mol^{-1}$) (Figure S2 and S3) are observed for H_2**L1**. These bands are only weakly affected by addition of KOH, deprotonating the phenolic OH groups. Interestingly, an absorption band at around 420 nm (ε = 2000 $L{\cdot}cm^{-1}{\cdot}mol^{-1}$), absent in the spectrum of the neutral ligand, is clearly visible when 2 equivalents of KOH are added to H_2**L1** (Figure S3). As for the absorption spectra of the

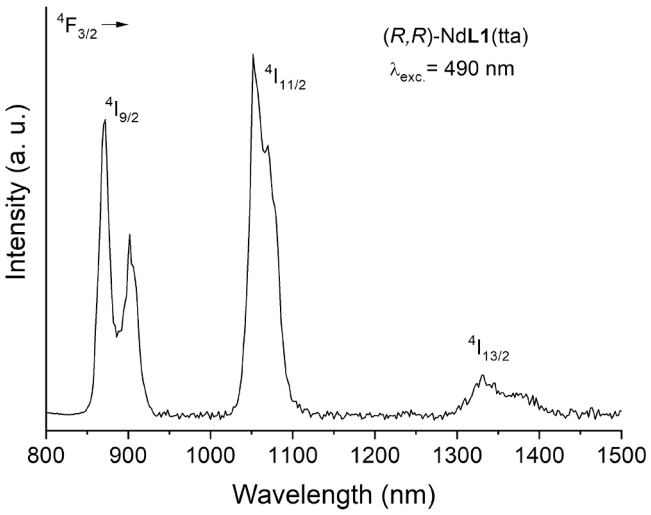

Fig. 6. Luminescence emission spectrum of (*R,R*)-Nd**L1**(tta) in the solid state at room temperature (λ_{exc} = 490 nm).

complexes (Figure S4), the higher energy UV component is slightly red shifted (around 264 nm) with respect to H_2**L1**, and two new strong bands are detected. One band is peaked at 294 nm (ε = 66500 $L{\cdot}cm^{-1}{\cdot}mol^{-1}$) and the other one around 341 nm (ε = 32300 $L{\cdot}cm^{-1}{\cdot}mol^{-1}$). Also in the visible range, we noticed differences between the spectra of the complexes and that of the deprotonated **L1** ligand (H_2**L1** + 2 equiv. KOH = K_2**L1**). In particular, in the case of (*R,R*)-Nd**L1**(tta) complex, an absorption band similar to the one observed for K_2**L1** is detected. In fact, the Nd-associated band, while broader, peaks at around 430 nm and shows a ε_{max} value of about 2000 $L{\cdot}cm^{-1}{\cdot}mol^{-1}$ (1844 $L{\cdot}cm^{-1}{\cdot}mol^{-1}$), like for K_2**L1** (Fig. 7). On the contrary, in the case of (*R,R*)-Yb**L1**(tta) complex, a slightly weaker (ε = 1470 $L{\cdot}cm^{-1}{\cdot}mol^{-1}$) absorption band, peaking around 450 nm and extending up to 575 nm, is observed (Fig. 7).

Discussion

Firstly, the inspection of the luminescence excitation spectra of Yb**L1**(tta) and Nd**L1**(tta) reveals that, apart from the direct Nd(III) excitation in the NIR spectral region, a very broad range of wavelengths can be used to sensitize the *f-f* luminescence of both Ln(III) ions (UV light above 250 nm and Vis light up to 600–650 nm). This is not usual, in particular in the case of Yb(III), as discussed in the introduction of this paper. The precise nature of these bands can be determined considering the

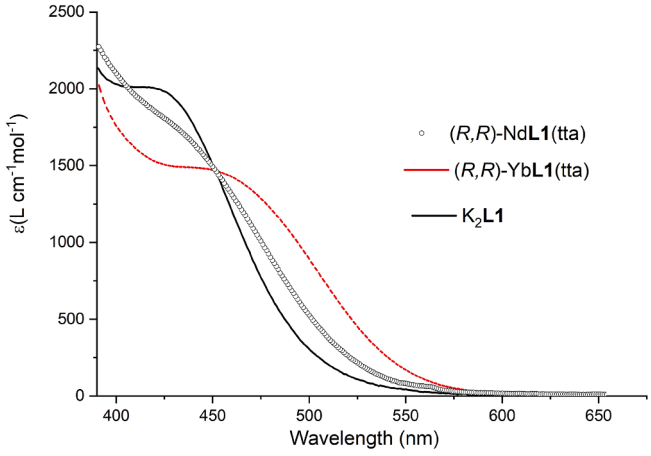

Fig. 7. Electronic absorption spectrum in the 390–650 nm range of (*R,R*)-K_2**L1**, (*R,R*)-Nd**L1**(tta) and (*R,R*)-Yb**L1**(tta) in ethanol solution (0.25 mM).

absorption features of both ligands surrounding the metal ion: 8-hydroxyquinolinate and tta. Regarding the latter, the two bands recorded in ethanol around 294 and 341 nm are related to the diketonate-centred singlet–singlet π-π* enolic transition [19]. The two bands located at around 260 nm and 305 nm are assigned to π → π * and n → π * transitions, respectively, of 8-hydroxyquinolinate, as already discussed in the literature [20] for ligands in which this heteroaromatic fragment is conjugated to an amide group. As also reported in this investigation, another component of the n → π * transition appears in the visible range (at around 420 nm) when the ligand is deprotonated. This absorption band is red-shifted when the ligand is coordinated to Ln(III) cations [20]. This is also what is observed for (*R,R*)-Yb**L1**(tta) and (*R,R*)-Nd**L1**(tta) complexes, even though in the case of the former this band is broader and red-shifted with respect to the Nd(III)-based counterpart (Fig. 7). The different absorption features of the two complexes in this spectral region suggest the presence of a band of a different nature for (*R,R*)-Yb**L1**(tta). Since Yb(III) is the most readily reduced ion in the Ln(III) series (with a reduction potential of −1.05 V *vs* NHE [21]), one electron of the 8-hydroxyquinolinate ligand can be transferred to the metal ion, giving rise to a ligand-to-metal charge transfer (LMCT) transition in the absorption spectrum of the complex. The related band, that should be weaker or absent in the case of the (*R,R*)-Nd**L1**(tta) complex, can account for the different color of the two powdered samples: (*R,R*)-Nd**L1**(tta) is orange while (*R,R*)-Yb**L1**(tta) is red (Figure S1). This band seems responsible for the extension of the excitation spectrum of the solid (*R,R*)-Yb**L1**(tta) complex up to 650 nm.

To sum up, several absorption bands of the H_2**L1** and tta ligands are involved in the sensitization of Yb(III) and Nd(III) luminescence. We can speculate that, in the case of Nd(III), upon excitation of tta (through the π-π* enolic transition, in the UV region) and 8-hydroxyquinolinate [conjugated to an imine function (through the π → π * and *n* → π * transitions, in the UV–vis region)] a Ligand-to-metal energy transfer (LMET or *antenna effect*) process occurs populating the Nd(III) excited levels above the $^2H_{11/2}$ state (see excitation spectrum in Fig. 5). On the other hand, in the case of Yb(III) energy levels above 10000 cm^{-1} (below 1000 nm) are not possible and the large energy mismatch between $^2F_{5/2}$ level and the excited states of the ligands prevents the involvement of a classical LMET phenomenon. Presumably, the LMCT level is crucial for the transfer of the excitation energy to the metal ion, with a mechanism similar to the one depicted in the Figure S5 and described in detail in the reference [17]. This level can be directly populated upon excitation around 450–500 nm or can be fed by the singlet and triplet excited states belonging to π → π * and *n* → π * transitions of the ligands.

As for the luminescence lifetime of the Yb(III) $^2F_{5/2}$ excited state, the recorded value [9.63(7) μs] is characteristic of an efficient light emission by hydrophobic metal complexes where no water molecules are present both in the inner and outer coordination spheres, thus hampering MPR process [22,23]. However, the presence of the C—H vibrations in the ligands appears to affect the luminescence efficiency and the values of lifetimes.

Conclusions

In this contribution, a detailed spectroscopic study on powdered samples of two heteroleptic and chiral complexes of Nd(III) [(Nd**L1**(tta)] and Yb(III) [Yb**L1**(tta)] was performed. The chromophoric ligands (the bidentate diketonate tta and a polydentate ligand containing 8-hydroxyquinolinate conjugated to an imine function; H_2**L1**) can efficiently sensitize the *f-f* Nd(III)-centered luminescence by a LMET process (*antenna effect*) involving a broad UV/Vis spectral range (250–600 nm). Similarly, the Yb(III) luminescence in Yb**L1**(tta) is sensitized upon excitation in a range of wavelengths which spans 400 nm (from 250 to 650 nm). Interestingly, in this case a LMCT level seems to play a leading role in the population of the $^2F_{5/2}$ excited state of Yb(III). We can hypothesize that this level possesses a dual role: *i)* it can transfer the excitation energy to $^2F_{5/2}$ and *ii)* it can be populated by the singlet and triplet excited states belonging to π → π * and *n* → π * transitions of both ligands. The here reported very interesting spectroscopic properties, like the NIR emission and the excitation located in a broad spectral range including the visible, can find possible applications in the biological and technological fields. For example, the downshifting ability of the complexes could be exploited in the solar energy area.

Declaration of Competing Interest

The authors declare that they have no known competing financial interests or personal relationships that could have appeared to influence the work reported in this paper.

Acknowledgements

The authors thank the Italian Ministry of University and Research for the received funds (PRIN (Progetti di Ricerca di Rilevante Interesse Nazionale) project "CHIRALAB", grant no. 20172M3K5N). FP, SR, SM, CN and MB gratefully also thank the Facility "Centro Piattaforme Tecnologiche" of the University of Verona for access to the Fluorolog 3 (Horiba-Jobin Yvon) spectrofluorometer and to the 600 MHz Bruker Avance III NMR spectrometer. Funding from the Universities of Verona and Parma is gratefully acknowledged.

Appendix A. Supplementary data

Supplementary data to this article can be found online at https://doi.org/10.1016/j.rechem.2022.100388.

References

[1] K. Dong, E. Ju, N. Gao, Z.Z. Wang, J.S. Ren, X.G. Qu, Synergistic eradication of antibiotic-resistant bacteria based biofilms in vivo using a NIR-sensitive nanoplatform, Chem Commun 52 (2016) 5312–5315, https://doi.org/10.1039/C6CC00774K.
[2] A.J. Amoroso, S.J.A. Pope, Using lanthanide ions in molecular bioimaging, Chem. Soc. Rev. 44 (2015) 4723–4742, https://doi.org/10.1039/C4CS00293H.
[3] M.C. Heffern, L.M. Matosziuk, T.J. Meade, Lanthanide probes for bioresponsive imaging, Chem. Rev. 114 (2014) 4496–4539, https://doi.org/10.1021/cr400477t.
[4] K. Kim, M. Lee, H. Park, J.H. Kim, S. Kim, H. Chung, K. Choi, I.S. Kim, B.L. Seong, I. C. Kwon, Cell-permeable and biocompatible polymeric nanoparticles for apoptosis imaging, J. Am. Chem. Soc. 128 (2006) 3490–3491, https://doi.org/10.1021/ja057712f.
[5] J.-C.-G. Bünzli, On the design of highly luminescent lanthanide complexes, Coord. Chem. Rev. 293–4 (2015) 19–47, https://doi.org/10.1016/j.ccr.2014.10.013.
[6] E. Cavalli, C. Nardon, O.G. Willis, F. Zinna, L. Di Bari, S. Mizzoni, S. Ruggieri, S. C. Gaglio, M. Perduca, C. Zaccone, A. Romeo, F. Piccinelli, NIR Circularly Polarized Luminescence from water stable organic nanoparticles containing a chiral Yb(III) complex, Chem. Eur. J. (2022), https://doi.org/10.1002/chem.202200574.
[7] P.A. Tanner, L. Zhou, C. Duan, K.L. Wong, Misconceptions in electronic energy transfer: bridging the gap between chemistry and physics, Chem. Soc. Rev. 47 (2018) 5234–5265, https://doi.org/10.1039/C8CS00002F.
[8] A. Brandner, T. Kitahara, N. Beare, C. Lin, M.T. Berry, P.S. May, Luminescence Properties and Quenching Mechanisms of $Ln(Tf_2N)_3$ Complexes in the Ionic Liquid bmpyr Tf_2N, Inorg. Chem. 50 (2011) 6509–6520, https://doi.org/10.1021/ic102538m.
[9] J.-C.-G. Bünzli, S.V. Eliseeva, Photophysics of lanthanoid coordination compounds, in: Comprehensive Inorganic Chemistry II (Second Edition): From Elements to Applications, Elsevier, 2013, pp. 339–398, 10.1016/B978-0-08-097774-4.00803-2.
[10] D.L. Dexter, A Theory of Sensitized Luminescence in Solids, J. Chem. Phys. 21 (1953) 836–850, https://doi.org/10.1063/1.1699044.
[11] G.H. Dieke, H.M. Crosswhite, H. Crosswhite, Spectra and Energy Levels of Rare Earth Ions in Crystals, Wiley Interscience, New York, 1968.
[12] W.T. Carnall, G.L. Goodman, K. Rajnak, R.S. Rana, A systematic analysis of the spectra of lanthanides doped into single crystal LaF_3, J. Chem. Phys. 90 (1989) 3443–3457, https://doi.org/10.1063/1.455853.
[13] W.D. Horrocks Jr., J.P. Bolender, W.D. Smith, R. Supkowski, Photosensitized near infrared luminescence of ytterbium(III) in proteins and complexes occurs via an internal redox process, J. Am. Chem. Soc. 119 (1997) 5972–5973, https://doi.org/10.1021/ja9644211.
[14] C. Reinhard, H. Güdel, High-resolution optical spectroscopy of $Na_3Ln(dpa)_3{\cdot}13H_2O$ with Ln = Er^{3+}, Tm^{3+}, Yb^{3+}, Inorg. Chem. 41 (2002) 1048–1055, https://doi.org/10.1021/ic0108484.
[15] V.A. Ilichev, A.V. Rozhkov, R.V. Rumyantcev, G.K. Fukin, I.D. Grishin, A. V. Dmitriev, D.A. Lypenko, E.I. Maltsev, A.N. Yablonskiy, B.A. Andreev, M. N. Bochkarev, LMCT facilitated room temperature phosphorescence and energy

transfer in substituted thiophenolates of Gd and Yb, Dalton Trans. 46 (2017) 3041–3050, https://doi.org/10.1039/C6DT04519G.
[16] A. Masuya-Suzuki, S. Goto, T. Kambe, R. Karashimada, Y. Kubota, N. Iki, Short radiative lifetime and non-triplet sensitization in near-infrared-luminescent Yb(III) complex with tripodal schiff base, ChemistryOpen 10 (2021) 46–55, https://doi.org/10.1002/open.2020002.
[17] Y.-J. Liang, F. Liu, Y.-F. Chen, X.-J. Wang, K.-N. Sun, Z. Pan, New function of the Yb^{3+} ion as an efficient emitter of persistent luminescence in the short-wave infrared, Light Sci. Appl. 5 (2016) e16124.
[18] E. Kasprzycka, A.N. Carneiro Neto, V.A. Trush, O.L. Malta, L. Jerzykiewicz, V. M. Amirkhanov, J. Legendziewicz, P. Gawryszewska, Spectroscopic aspects for the Yb^{3+} coordination compound with a large energy gap between the ligand and Yb^{3+} excited states, Spectrochim. Acta A Mol. Biomol. Spectrosc. 274 (2022), 121072, https://doi.org/10.1016/j.saa.2022.121072.
[19] T. Sekine, A. Hokura, I. Tanaka, Rate and equilibrium of the distribution of 2-thenoyltrifluoroacetone in carbon tetrachloride-aqueous perchlorate solution systems, Anal. Sci. 12 (1996) 747–753, https://doi.org/10.2116/analsci.12.747.
[20] S. Comby, D. Imbert, C. Vandevyver, J.-C.-G. Bünzli, A novel strategy for the design of 8-hydroxyquinolinate-based lanthanide bioprobes that emit in the near infrared range, Chem. Eur. J. 13 (2007) 936–944, https://doi.org/10.1002/chem.200600964.
[21] A.J. Bard, R. Parsons, J. Jordan, Standard Potentials in aqueous solution, Marcel Dekker Inc, New York, 1985.
[22] G. Brito-Santos, B. Gil-Hernández, I.R. Martín, R. Guerrero-Lemus, J. Sanchiz, Visible and NIR emitting Yb(III) and Er(III) complexes sensitized by β-diketonates and phenanthroline derivatives, RSC Adv. 10 (2020) 27815–27823, https://doi.org/10.1039/D0RA05539E.
[23] N.M. Shavaleev, S.J.A. Pope, Z.R. Bell, S. Faulkner, M.D. Ward, Visible-light sensitisation of near-infrared luminescence from Yb(III), Nd(III) and Er(III) complexes of 3,6-bis(2-pyridyl)tetrazine, Dalton Trans. (2003) 808–814, https://doi.org/10.1039/B300294B.